Automatic Path Generation for Multirotor Descents Through Varying Air Masses above Ascension Island

Colin Greatwood*, Tom Richardson† and Jim Freer‡
University of Bristol, Bristol, UK
Rick Thomas§
University of Birmingham, Birmingham, UK
Rebecca Brownlow, David Lowry, Rebecca E. Fisher, Euan G. Nisbet¶
Royal Holloway, University of London, London, UK

As part of a NERC funded project investigating the southern methane anomaly a team drawn from the Universities of Bristol, Birmingham and Royal Hollaway flew three large multirotors from Ascension Island for the purposes of atmospheric sampling. The core objective of these flights was to collect air samples from below, within and above the trade wind inversion layer.

The sampling missions required the aircraft to ascend vertically to collect samples from altitudes up to 2.5km above ground level. The descent on the return journey required careful consideration as rotary wing vehicles can become unstable when descending vertically through still air. The wind profiles over the altitudes flown above Ascension varied from persistent strong winds to areas of very still air.

This paper describes a method for estimating wind speed and direction from the multirotor's attitude during the ascent. An optimization process for determining ideal descent profiles is also presented, which allows the operator to approve automatically generated flight profiles during flight, just prior to the descent. The descent profiles enable the multirotor vehicle to avoid descending vertically through still air by commanding a horizontal translation. Horizontal deviations are minimised in order to avoid additional energy expenditure.

I. Introduction

There is currently a great deal of interest in the origin of a concentration of methane observed in the southern hemisphere. Leading the ongoing work in this area, NERC (Natural Environment Research Council, UK) funded a project entitled Investigation of the Southern Methane Anomaly: causes, implications, and relevance to past global events. The Universities of Bristol and Birmingham, as part of this project were asked to collect air samples using a Small Unmanned Air System (SUAS), above the inversion layer on Ascension Island for the purposes of identifying methane concentrations and isotopic composition. In September 2014 over sixty flights were carried out over a period of ten days and to altitudes up to 2.5km above ground. This paper describes how the wind profile varied over these altitudes due to the location of different air masses. Careful consideration of the flight profiles was required to ensure the safety of the vehicle when passing through different wind conditions.

The ideal flight path for the octocopter from a mission scripting perspective would be to ascend vertically to the required altitude, collect the air sample and then descend back along the same path to the take off site. This flight profile, however, can cause problems for rotary wing vehicles in still air conditions due to

*Research Associate, Department of Aerospace Engineering. Email Colin.Greatwood@bristol.ac.uk
†Senior Lecturer, Department of Aerospace Engineering. Email Thomas.Richardson@bristol.ac.uk, Senior Member AIAA.
‡Professor, School of Geographical Sciences. Email Jim.Freer@bristol.ac.uk
§Senior Research Fellow, School of Geography, Earth & Environmental Sciences. Email R.thomas@bham.ac.uk
¶Professor of Earth Sciences. Email euan.nisbet@gmail.com

the potential to enter a vortex ring state.[1,2] The vortex ring state is a highly undesirable flight state during which the flow around the rotor has large amounts of recirculation and turbulence. The vertical descent velocity during the vortex ring state is hard to control and low frequency vibration may be experienced by the vehicle.

The wind speeds on Ascension Island were typically around $8m/s$ at ground level. It would therefore be reasonable for the octocopter to descend vertically through these conditions as the horizontal airspeed would be high enough to avoid entering the vortex ring state. The wind conditions throughout and above the inversion layer, however, were not so consistent. Above the inversion layer the vehicle entered a new air mass that could have a greater or lower wind speed to that experienced on the ground. If the wind speed was reduced then a vertical descent profile may not be desirable, whilst if the wind speed was seen to increase then a vertical descent may be suitable. The flight profile should therefore be adjusted to include horizontal translations in order to control the airspeed experienced during descent.

Due to lack of regional observations, atmospheric models for Ascension island could potentially struggle to resolve the local wind field with high enough accuracy for the flight planning described in this paper. Therefore, producing ideal descent profiles can be separated into two problems: 1. Determining the wind conditions; and 2. generating descent profiles that minimize energy expenditure of the UAV.

Researchers have previously studied methods for determining wind conditions in real-time. Predominantly work in this area has focussed on characterising the wind in order to reject disturbances or improve state estimation. Arain and Kendoul installed a pitot-static system onboard their octocopter[3] in order to measure the airspeed directly and augment the flight controller to reject wind disturbances. Baranek and Solc investigated[4] the effects of wind disturbances on internal attitude estimates. Schiano et al. discussed the estimation of wind effects on a quadrotor with no additional sensors and performed experiments in a wind tunnel,[5] leading to results that could be used to improve aerodynamic models. Waslander and Wang have simulated these wind effects on a small quadrotor[6] and show how a wind estimate can be used to improve positional accuracy that would allow operation close to obstacles.

There are two main contributions in this paper, the first in Section III describes how the wind speed and direction can be estimated from the UAV's attitude using experimental data. Secondly, an optimization process is presented in Section V that parametrizes the wind profiles and generates descent profiles for minimizing energy expenditure.

Nomenclature

$v_a(h)$	Estimated horizontal (2D) airspeed observed by the vehicle
$\hat{v}_a(h)$	Expected horizontal (2D) airspeed observed by the vehicle during descent
$v_g(h)$	Horizontal (2D) ground speed of the vehicle
$\hat{v}_g(h)$	Planned horizontal (2D) ground speed of the vehicle during descent
$v_w(h)$	Estimated horizontal (2D) wind speed
$\hat{v}_w(h)$	Parametrised estimated horizontal (2D) wind speed
h	Altitude above ground level
$h_{\max}$	Maximum altitude reached during flight
$(x(i), y(i), z(i))$	Location of waypoint i on descent profile

II. Platform Description

The aircraft used on the sampling campaign was an eight motor multirotor (or octocopter) in an "X-8" configuration, shown in Figure 1(a). The airframe is a custom design from the University of Bristol that provides enough space for a large battery capacity (typically 533Wh, but tested with up to 710Wh) and air sampling equipment. The autopilot and electronics are all off the shelf components. A summary of the vehicle specifications is given in Table 1.

An eight rotor configuration was chosen to achieve reasonable redundancy against loss of a motor or speed controller during flight. The vehicle could theoretically sustain a loss of four motors, provided that none were on the same arm, and tests on disconnecting three motors demonstrated that the vehicle retained good control in flight. Other user reports of octocopter platforms have anecdotally suggested that the four arm coaxial configuration was likely to provide better gust tolerance than a flat eight arm configuration. It

was found that the vehicle did indeed perform well in the wind, but further research is being conducted at the University of Bristol in order to quantify the differences between motor layout configurations.

(a) X-8 Multirotor

(b) Ground support

Figure 1. Unmanned Aircraft System

Maximum Take Off Weight (inc. batteries)	10kg
Diagonal rotor-rotor distance	1.07m
Maximum battery capacity	32,000mAh 6 cell Lithium Polymer
Motors	T-Motor MN3515 400KV
Propellers	T-Motor 16x5.4"
Electronic Speed Controllers	RCTimer NFS ESC 45A (OPTO)
Autopilot	Pixhawk by 3DRobotics
Autopilot software	ArduCopter v3.1.5
Safety pilot control link	FrSky L9R 2.4GHz
Ground Control Station link	Ubiquiti 5GHz directional
Onboard computing	BeagleBone Black
Sampling pump	KNF Diaphragm Pump (NMP 850 KNDC)

Table 1. Key UAV specifications

III. Wind Estimation

This section describes the method by which the wind speed and direction can be estimated by observing the octocopter's attitude. Figure 2(a) shows the forces acting on the Unmanned Air Vehicle (UAV), where the component of lift (L) produced by the aircraft in the vertical direction to maintain altitude may be described by

$$L = mg \tag{1}$$

where m is the mass of the aircraft and g is acceleration due to gravity. The total thrust produced by the vehicle (T) can therefore be described as a function of the total bank angle γ, which is calculated from the magnitude of the roll (θ) and pitch (ϕ) angles,

$$T = \frac{L}{\cos(\gamma)} \tag{2}$$

$$T = \frac{mg}{\cos(\gamma)} \tag{3}$$

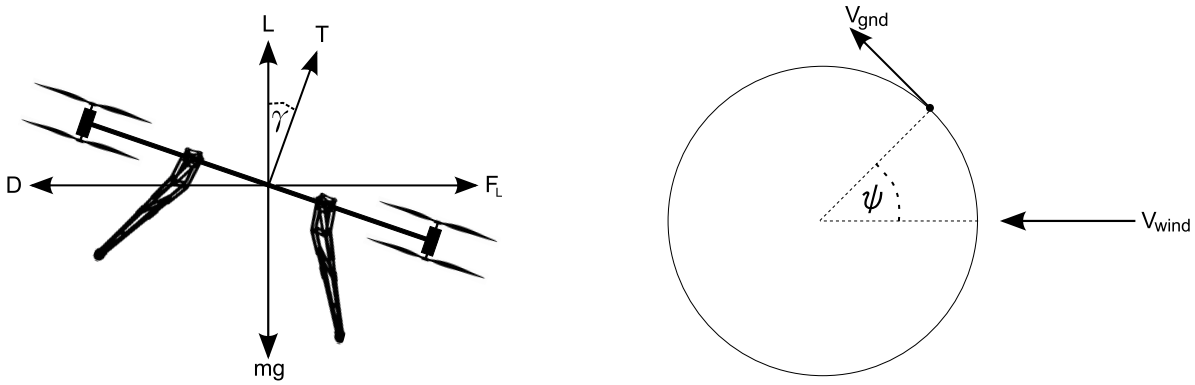

(a) Free body diagram of forces on UAV

(b) Angle around track during orbit manoeuvre

Figure 2. Forces, angles and velocities used for wind estimation

The lateral thrust produced (F_L) will therefore be

$$F_L = T\sin(\gamma) \tag{4}$$

$$F_L = \frac{mg}{cos(\gamma)}\sin(\gamma) \tag{5}$$

$$F_L = mg\tan(\gamma) \tag{6}$$

A steady state velocity into wind will be achieved when the lateral thrust F_L equals the drag D. Assuming that the main component of drag on the vehicle will be parasitic drag,[7] then

$$D \propto v_{asp}^2 \tag{7}$$

$$\therefore D = \kappa v_{asp}^2 \tag{8}$$

where v_{asp} is the airspeed observed by the vehicle, hence

$$v_{asp} = \sqrt{\frac{D}{\kappa}} \tag{9}$$

$$= \sqrt{\frac{F_L}{\kappa}} \tag{10}$$

$$= \sqrt{\frac{mg\tan(\gamma)}{\kappa}}, \tag{11}$$

$$\forall\gamma \in \left[0, \frac{\pi}{2}\right) \tag{12}$$

The airspeed can therefore be deduced from the aircraft's total bank angle γ once the parameter κ has been identified. A constant altitude, constant ground-speed flight was performed around a circular path with a 150 metre radius. The total bank angle is shown in Figure 3. A sine wave was fitted to the bank angle in the plot as the estimated bank angle required to maintain the commanded $3m/s$ ground speed over the course of the circular manoeuvre.

The airspeed as observed by the UAV over the circular manoeuvre is the result of the wind speed and ground speed as depicted in Figure 2(b). Assuming both the wind direction and ground speed remain constant for the duration of the experiment, the airspeed is a function of the vehicle's position in the orbit,

$$v_{asp} = v_{wind} - v_{gnd}\cos\left(\frac{\pi}{2} - \psi\right) \tag{13}$$

where ψ represents the UAV's position relative to the wind vector. The direction of the wind speed vector can be estimated from the sine wave fitted to the bank angle shown in Figure 3, where the bank angle is

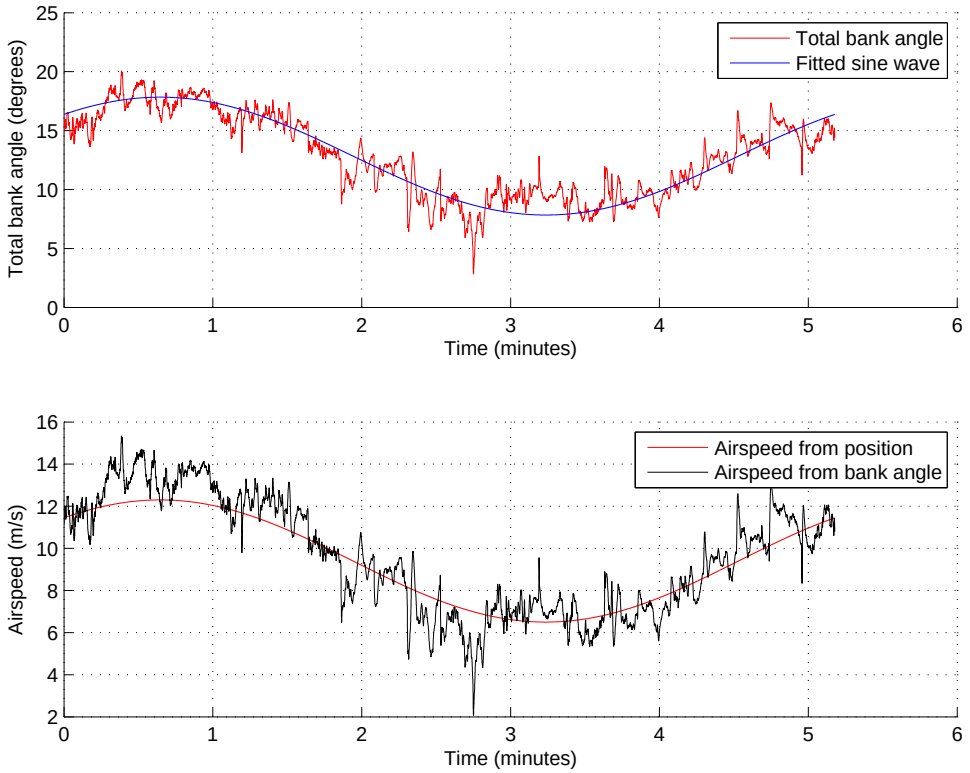

Figure 3. Airspeed estimation from bank angle and position around circular orbit

maximum at $\psi = 3\pi/2$ and minimum at $\psi = \pi/2$. The mean wind speed during the orbit manoeuvre was measured to be $9.4m/s$ and the ground speed as $3m/s$, hence the airspeed as a function of position can be found from Eqn. 13. The unknown parameter κ in Eqn. 11 can therefore be found by fitting the bank angle data to the to the airspeed curve as shown in Figure 3 where $\kappa = 1.99$.

An experiment was carried out using a sonic anemometer to measure the wind speed at 4m AGL whilst the UAV hovered at the same altitude a few metres down-wind. Over the duration of the three minute hover the wind speed and direction average and standard deviations were as estimated using the above equations. The estimated and measured values from the experiment are summarized in the following table, demonstrating good correlation.

	Wind Speed		Wind Direction	
	Mean (m/s)	Standard Deviation	Mean (degrees)	Standard Deviation
Measured	7.00	2.51	294.7	20.1
Estimated	6.51	3.00	301.0	31.4

Table 2. Comparison between estimated and measured wind speed during hover

During vertical ascents, rather than circular orbits, the wind direction may be estimated directly from the magnitude of roll and pitch angles as the ground speed is zero. The wind speed is estimated from Equation 11 using the identified value of κ.

III.A. Wind Estimation in Vertical Flight

A flight was performed with the octocopter ascending up to 1800m AGL and back again in a straight line. The ground speed was negligible, hence the roll and pitch attitudes observed were required solely for overcoming the wind in order to maintain the commanded horizontal position. Figure 4(a) shows the total bank angle (γ) of the vehicle for both the ascent and decent. The vertical speed was fixed to $5m/s$ in both directions and it can be seen that this has an affect on the bank angle required to overcome the wind - assuming that the wind

conditions did not vary significantly over the duration of the fifteen minute flight. The bank angle difference appears to be roughly two degrees difference between the ascent and descent. A rough approximation has therefore been made that ascending at $5m/s$ will increase the total bank angle by one degree, and descending will decrease it by the same. Further analysis, which is not conducted here, on different ascent and descent rates within different wind conditions may provide a more accurate approximation.

By subtracting a degree from the total bank angle observed during the ascent, an equivalent total bank angle was approximated for what would be required for a stationary hover. This adjusted total bank angle can then be used to estimate the windspeed using the equations from the previous section. The estimated windspeed for the flight to 1800m is shown in Figure 4(b). The windspeed above 1350m AGL was quite slow, reaching less that $2.5m/s$ at times. The effect that this low windspeed had on the attitude during the descent is apparent in Figure 4(a) where the aircraft rocked noticeably until it reached faster moving air. This rocking is due to the instabilities caused when the vehicle descends into its own wake, which provides the key motivation for generating trajectories that include horizontal displacements during descent through still air.

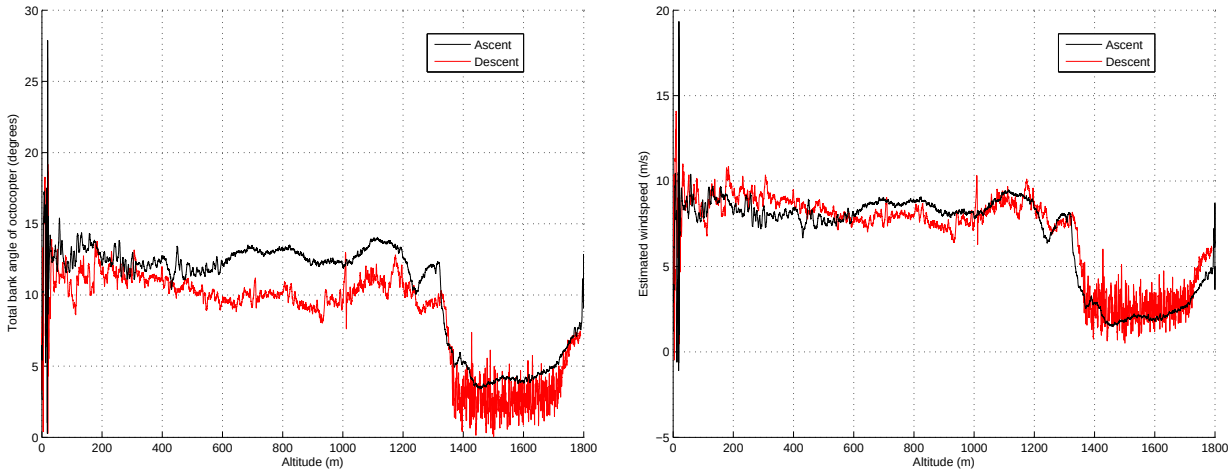

(a) Total bank angle during ascent and descent

(b) Estimated windspeed during ascent and descent

Figure 4. Estimated windspeeds from aircraft attitude during flight to and from 1800m AGL

IV. Flight Safety

As shown in Figure 4(a), descending vertically during close to still air conditions can cause significant rocking as the flight controller attempts to hold the vehicle level during this unstable flight state. In this particular example the rocking is bounded and hence does not necessarily pose an immediate risk to the safety of the vehicle. The ongoing hunting that the motors are forced to perform to maintain stability, however, does cause the aircraft to consume more power, which in turn reduces the flight endurance. A reduction in endurance can become a safety risk, especially so if the magnitude is unknown prior to take off. One must identify how much endurance will be lost due to the height of the slow moving air to ensure enough endurance is available for a safe and controlled landing. This endurance may be estimated by performing sequential flights up to increasing altitudes and measuring the remaining battery charge upon landing. By using the approach presented by this paper, however, the endurance may be improved by including horizontal displacements in the descent profile to avoid descending vertically through still air masses.

Another potential issue related to budgeting the available power is flight through fast moving air. Even when descending, the fast moving air will require the aircraft to work hard to follow the flight profile and again reduce the endurance. The method presented in the following section describes how to take advantage of the differing air masses and their wind directions. The descent profiles are planned in order to minimize the effective airspeed throughout the descent, whilst still keeping it above safe levels.

Wind conditions will not necessarily always be known in advance. A prudent flight operator would therefore monitor the conditions throughout the flight to ensure that the aircraft both remains within its flight envelope, but also has a good estimate of the available energy to ensure a safe descent. The flights

conducted on Ascension Island were always planned such that an expected 20% or more battery power would always be left. This not only provides a buffer for errors in estimating endurance, but also improves the longevity of the battery packs themselves.

Another key safety consideration is the location over which the aircraft flies. The team conducting the flight operations carefully picked the launch and recovery site. The site was secluded and the nearby road was shut in order to prohibit traffic passing underneath the flight paths. A horizontal movement away from the operators was undertaken prior to the ascent; in the unlikely event of a complete system failure (*i.e.* the aircraft free falling) no persons or property would be affected. Testing proved the terminal velocity of the vehicle to be $20m/s$. By taking into account the wind speed and direction a good estimate of the likely areas that the vehicle could land from a free fall can be calculated. From the flight profiles planned up to the cleared ceiling of $10,000$ feet the team were able to confirm the reachable zone below would be clear. The automatic waypoint generation described here should also be constrained in order to maintain safe separation from persons not under the control of the operators.

V. Descent Profile Generation

The key motivation behind automatically generating descent profiles is to ensure the aircraft does not descend vertically into its own wake. The profiles may be tuned by hand, but an algorithm for automatically generating the paths would enable faster operations and potentially create more efficient trajectories. From testing, it was found that the octocopter did not experience instabilities when translating horizontally at velocities greater than or equal to the descent rate during still air conditions. Practically, this means that the desired horizontal airspeed of the vehicle should be greater than $5m/s$ given the commanded $5m/s$ descent rate. In strong enough winds this does mean that vertical descents would be acceptable. In low winds the vehicle must translate horizontally in order to increase the airspeed $v_a(h)$, given by

$$v_a(h) = v_w(h) - v_g(h) \tag{14}$$

where $v_w(h)$ is the windspeed and $v_g(h)$ is the groundspeed of the octocopter for a given height h above ground.

V.A. Windspeed Parametrisation

In order to simplify the descent profile design the wind speed and direction are parametrised by altitude. The estimated wind profile was split into 50 metre vertical sections as the inversion layer was not observed to be shorter than this during the campaign. The parametrised wind speed is calculated at the interface of each of the n^h vertical sections as follows

$$\hat{h}(i) = i \times 50 \tag{15}$$

$$\hat{v}_w(1) = \overline{v_w(h)}, \quad 0 \leq h \leq 25 \tag{16}$$

$$\hat{v}_w(n^h) = \overline{v_w(h)}, \quad \hat{h}(n^h) - 25 \leq h \leq \hat{h}(n^h) \tag{17}$$

$$\hat{v}_w(i) = \overline{v_w(h)}, \quad \hat{h}(i) - 25 \leq h \leq \hat{h}(i) + 25 \tag{18}$$

$$\forall i \in \left[0..n^h\right]$$

where each discrete altitude is given by $\hat{h}(i)$ and $\overline{v_w(h)}$ represents the mean estimated windspeed over the given height intervals. The parametrised wind speed at any altitude h is therefore found by linearly interpolating between the two adjacent wind speeds $\hat{v}_w(i)$ and $\hat{v}_w(i+1)$, where $\hat{h}(i) \leq h \leq \hat{h}(i+1)$. The same method is used for parametrising the wind direction. The resulting parametrisation of the previous wind speed and direction estimates are shown in Figure 5, which shows good correlation.

V.B. Optimizing Lateral Displacements

The optimal descent profiles should minimise the energy expended by the octocopter in order to extend the endurance. As commanded lateral airspeed of the aircraft increases, so does the power required and so it is reasonable to attempt to minimise this. As previously identified, the ideal descent profiles would be constrained such that the lateral airspeed of the vehicle does fall below the vertical descent rate. Calculating

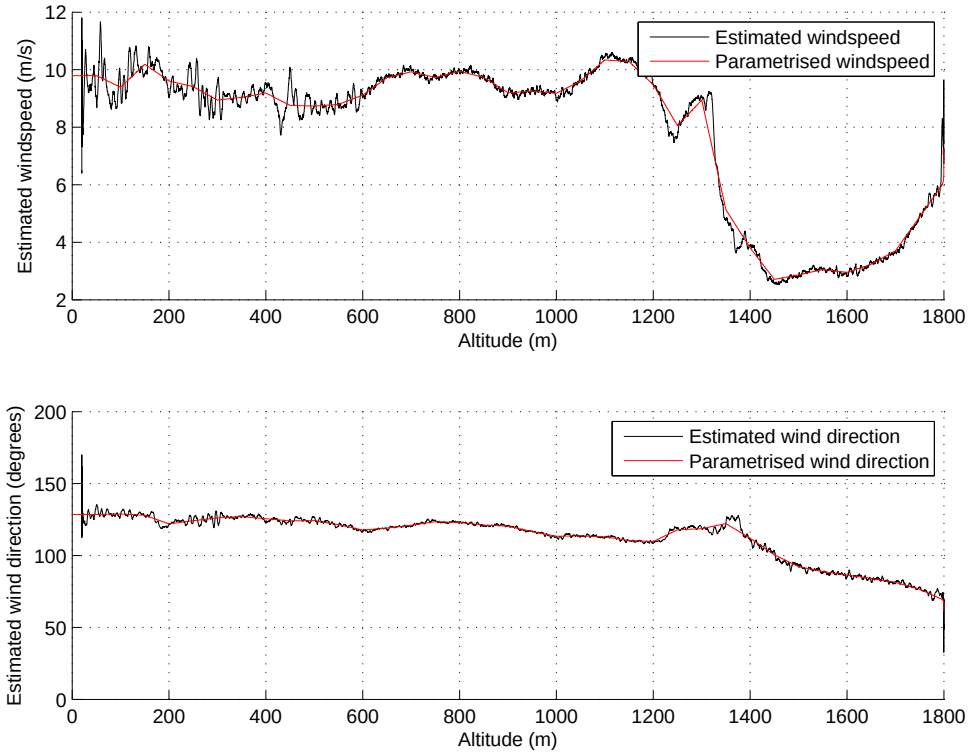

Figure 5. Wind speed and direction parametrisation for flight up to 1800m AGL

the descent profiles therefore becomes an optimisation problem where the lateral displacements during the descent are selected such that the airspeed is minimised subject to a minimum allowable constraint.

The wind parametrisation in the previous section provides a smoother and smaller dataset than the higher sample rate estimation data and so is used directly in the optimisation. The expected lateral airspeed during the descent $\hat{v}_a(h)$ is minimised by creating an additional $(n^{wp}-2)$ intermediate waypoints in the descent that lead to a non-zero ground speed. The optimisation problem is posed as follows and a Nelder-Mead[8] algorithm is used to solve it.

$$J = \min_{x(i),y(i),z(i)\forall i\in[1..n^{wp}]} \frac{1}{h_{\max}} \sum_{h=0}^{h_{\max}} \|\hat{v}_a(h)\| \tag{19}$$

$$\text{s.t. } \hat{v}_a(h) = \hat{v}_w(h) - \hat{v}_g(h) \tag{20}$$

$$\hat{v}_g(h) = \begin{pmatrix} \hat{v}_g^x(h) \\ \hat{v}_g^y(h) \end{pmatrix} \tag{21}$$

$$\hat{v}_g^x(h) = \frac{x(i+1)-x(i)}{z(i+1)-z(i)}$$

$$\hat{v}_g^y(h) = \frac{y(i+1)-y(i)}{z(i+1)-z(i)}$$

$$z(i) \le h \le z(i+1),\ \forall i \in [1..(n^{wp}-1)] \tag{22}$$

$$z(1) = 0 \tag{23}$$

$$z(n^{wp}) = h_{max} \tag{24}$$

$$\|\hat{v}_a(h)\| \ge v_z \forall h \in [0..h_{\max}] \tag{25}$$

The altitudes $z(i)$ along with $x(i)$ and $y(i)$ excursions are therefore determined by the optimisation process to control the ground speed and hence the expected airspeed observed by the octocopter in the descent. The constraint in (25) ensures that the airspeed is no smaller than the descent rate throughout the

trajectory. Constraining the horizontal speed to match or exceed the descent rate ensures the airspeed vector observed by the octocopter is no greater than 45° from the horizon, minimizing the chances of entering the vortex ring state.

An example result of the optimization is given in Figure 6 for the same 1800m AGL flight used in previous examples. The number of intermediate waypoints was set to two, *i.e.* $n^{wp} = 4$. The result shows that the expected descent speed would remain close to eight metres per second throughout the majority of the flight. During the transition between the two air masses the airspeed would vary, but remain safe. Figures 7-9 show the same descent profiles for different flights, demonstrating the ability of the algorithm to create reasonable profiles for varied wind conditions. Note the direction of the wind as observed by the vehicle is not optimised for, but is plotted for interest.

Perhaps the most intuitive altitude to place the waypoints would be at the locations at which the wind changes speed and direction, *i.e.* at the boundary of the air masses. This theory of placing the waypoints at the air mass boundaries is reinforced by the result of the profiles for flights A and D, shown in Figures 6 and 9. The optimiser found a different result, however, for flights B and C, shown in Figures 7 and 8. The $5m/s$ lateral airspeed constraint is active for flights B and C and so in this case the optimisation process has placed the waypoints at the locations where the expected airspeed meets the $5m/s$ constraint.

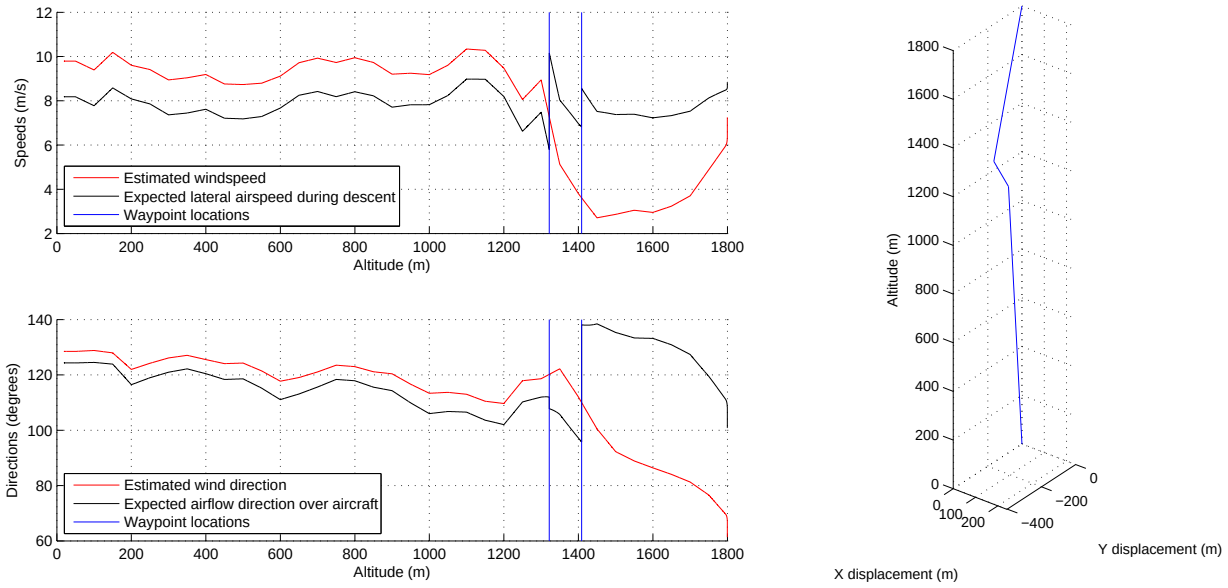

(a) Expected horizonatal airspeeds during descent

(b) Profile during descent

Figure 6. Optimized descent profile from 1800m AGL - Flight A

The optimizations take less than a second on a desktop computer, which means that they are suitable for computing during operations prior to commencing the descent. Once the operator has confirmed that he is happy with the profile then he can press upload to update the waypoints onboard the aircraft.

V.C. Flight Result with Horizontal Displacements

Another flight to 1800m AGL was undertaken, except this time some horizontal excursions were programmed into the descent in order to increase the horizontal airspeed through the calm upper winds. Figure 10 shows the current consumption throughout the two flights. It can be seen in the first flight that when descending through near-still air the current consumption is approximately the same as what is required to hover. Upon reaching approximately 1300m AGL, the current is seen to drastically drop to nearly half. This drop in current ties in exactly with the location where the wind speeds are shown to pick up in Figure 4(b). In the comparison flight (Fig. 10) the horizontal excursions enabled the aircraft to escape descending into its own wake. The resulting current draw is much more consistent throughout the descent, only spiking when the aircraft is required to change direction. Importantly, the mean current consumption is lower during the descent of the latter flight due to the routing of the return path.

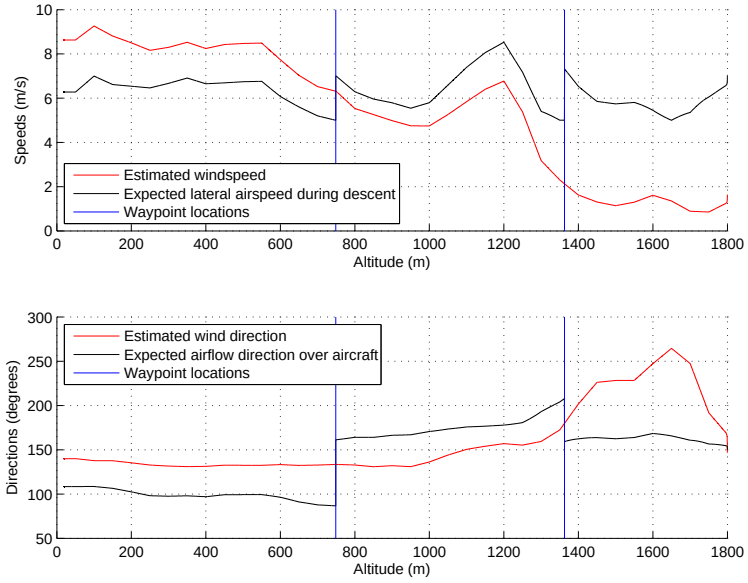

(a) Expected horizonatal airspeeds during descent

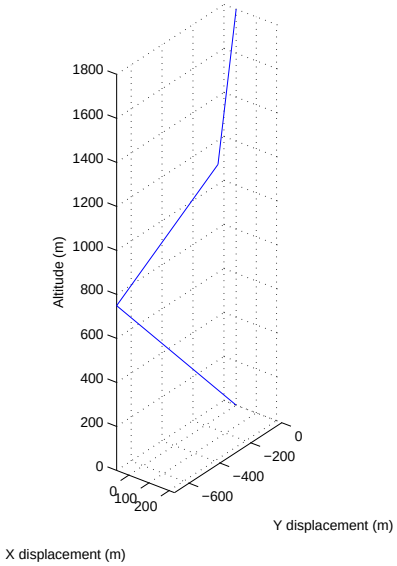

(b) Profile during descent

Figure 7. Optimized descent profile from 1800m AGL - Flight B

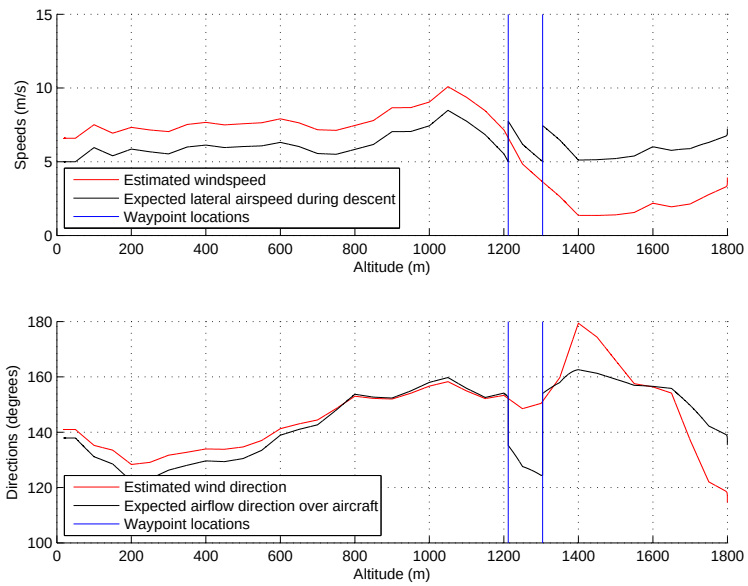

(a) Expected horizonatal airspeeds during descent

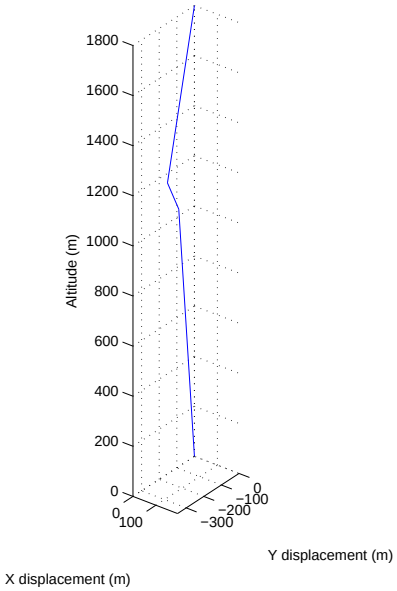

(b) Profile during descent

Figure 8. Optimized descent profile from 1800m AGL - Flight C

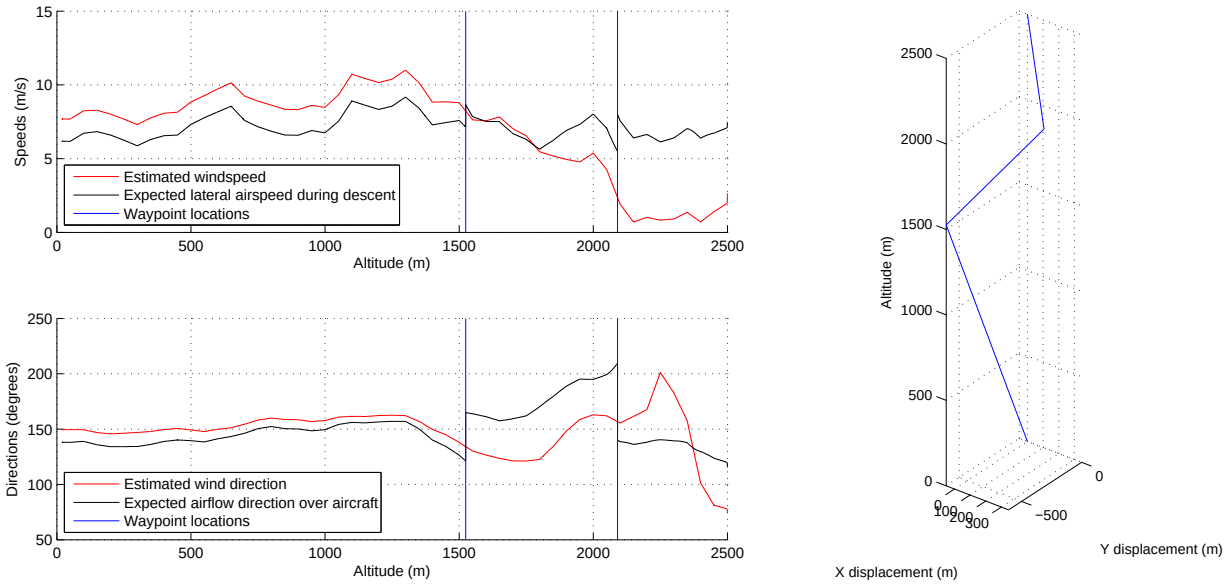

(a) Expected horizonatal airspeeds during descent

(b) Profile during descent

Figure 9. Optimized descent profile from 2500m AGL - Flight D

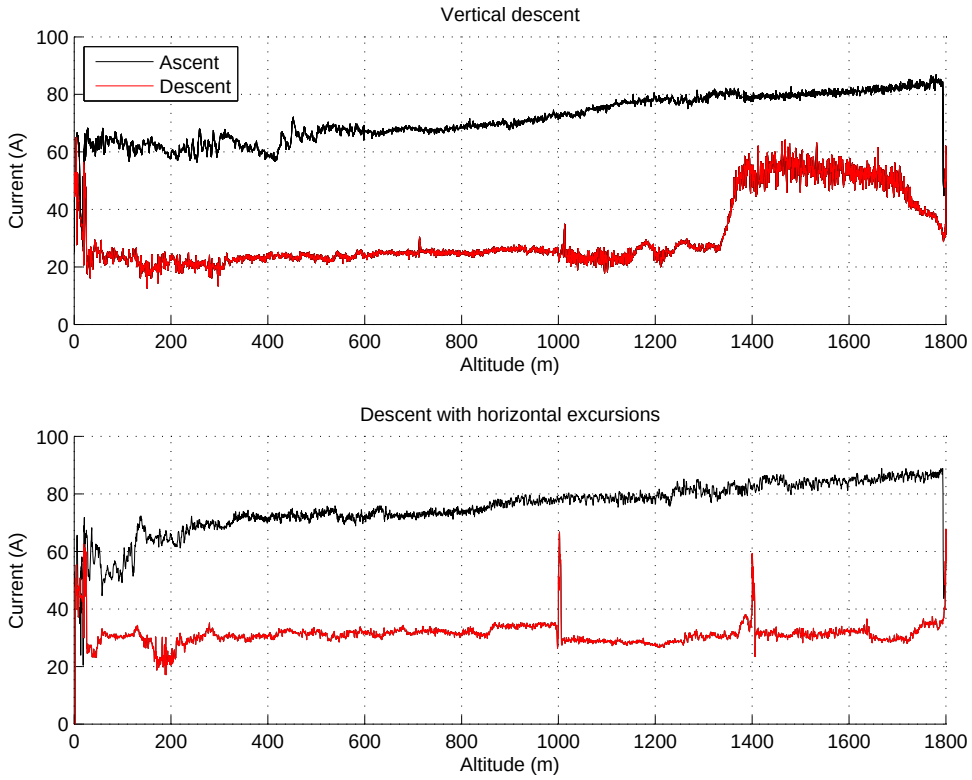

Figure 10. Two flights to 1800m AGL: First with vertical descent, second with horizontal excursion

VI. Conclusions

One of the challenges of flying rotary wing vehicles vertically to high altitudes is ensuring the safe descent through still or close to still air. Flight data has been presented here that shows the effects on a multirotor vehicle descending through its own wake in close to still air. The rocking observed increased the power consumption and could have impacts on flight safety if not carefully considered.

A method for determining the wind speed and direction from the vehicle's attitude is presented, using experimental data to identify the parameters. A simple parametrisation is presented for approximating the estimated wind speed and direction. The parametrised wind profile is then used to create optimal descent trajectories that include horizontal displacements for achieving minimal, but safe, horizontal airspeeds on the return journey. A result is included that demonstrates improved performance from planning a descent profile through near-still air.

Acknowledgements This work is supported by the Natural Environment Research Council Grant NE/K006185/1 Investigation of the Southern Methane Anomaly: causes, implications, and relevance to past global events.

References

[1]W. Johnson, *Helicopter Theory*. Courier Corporation, 1994.

[2]G. D. Padfield, *Helicopter Flight Dynamics*. Blackwell Publishing, 2007.

[3]B. Arain and F. Kendoul, "Real-time wind speed estimation and compensation for improved flight," *Aerospace and Electronic Systems, IEEE Transactions on*, vol. 50, pp. 1599–1606, April 2014.

[4]R. Baranek and F. Solc, "Model-based attitude estimation for multicopters," *Advances in Electrical and Electronic Engineering*, vol. 12, no. 5, 2014.

[5]F. Schiano, J. Alonso-Mora, K. Rudin, P. Beardsley, R. Siegwart, and B. Siciliano, "Towards estimation and correction of wind effects on a quadrotor uav," in *IMAV 2014: International Micro Air Vehicle Conference and Competition 2014, Delft, The Netherlands, August 12-15, 2014*, Delft University of Technology, 2014.

[6]S. L. Waslander and C. Wang, "Wind disturbance estimation and rejection for quadrotor position control," in *AIAA Infotech@ Aerospace Conference and AIAA Unmanned... Unlimited Conference, Seattle, WA*, 2009.

[7]J. D. Anderson, *Fundamentals of aerodynamics*. McGraw-Hill, Boston, Massachusetts, 2001.

[8]J. A. Nelder and R. Mead, "A simplex method for function minimization," *The computer journal*, vol. 7, no. 4, pp. 308–313, 1965.